Three-dimensional physics-based registration of pelvic system using 2D dynamic magnetic resonance imaging slices — Source link ⎆

Hadrien Courtecuisse, Zhifan Jiang, Olivier Mayeur, Olivier Mayeur ...+8 more authors

Institutions: French Institute for Research in Computer Science and Automation, university of lille, Centre national de la recherche scientifique

Related papers:

- Geometric Representation of the Pelvic Organs
- Bone motion analysis from dynamic MRI: acquisition and tracking.
- Deriving anatomical context from 4D ultrasound
- Stereoscopic 4D-Visualization of Craniofacial Soft Tissue based on Dynamic MRI and 256 Row 4D-CT
- 2D-3D Registration of Vascular Images

Three-dimensional physics-based registration of pelvic system using 2D dynamic magnetic resonance imaging slices

Hadrien Courtecuisse, Zhifan Jiang, Olivier Mayeur, Jean-Francois Witz, Pauline Lecomte-Grosbras, Michel Cosson, Mathias Brieu, Stéphane Cotin

HAL Id: hal-02873023
https://hal.inria.fr/hal-02873023

Submitted on 18 Jun 2020

FULL PAPER

3D Physics-based Registration of Pelvic System Using 2D Dynamic MRI Slices

H. Courtecuisse[1,2] | Z. Jiang[3] | O. Mayeur[4,5] | J.-F. Witz[4,5] | P. Lecomte[4,5] | M. Cosson[6,7] | M. Brieu[4,5] | S. Cotin[2]

[1] AVR/ICube Strasbourg, France, France
[2] Inria, Nancy, France
[3] Univ. Lille, UMR 9189 - CRIStAL - Centre de Recherche en Informatique Signal et Automatique de Lille, France
[4] Centrale Lille, Villeneuve d'Ascq, France
[5] CNRS, Lille, France
[6] CHU Lille, Service de Chirurgie Gynécologique, France
[7] Univ. Lille, Faculté de Médecine,France

Correspondence
*H. Courtecuisse, Email:
hcourtecuisse@unistra.fr

This paper introduces a method for dynamic 3D registration of female pelvic organs using 2D dynamic magnetic-resonance images (MRI). The aim is to provide a better knowledge and understanding of pathologies such as prolapsus or abnormal mobility of tissues. 2D dynamic MRI sequences are commonly used in nowadays clinical routines in order to evaluate the dynamic of organs, but due to the limited view, subjectivity related to human perception cannot be avoided in the diagnoses. A novel method for 2D/3D registration is proposed combining 3D Finite Element models with a priori knowledge of boundary conditions, in order to provide a 3D extrapolation of the dynamic of the organs observed in a single 2D MRI slice. The method is applied to the 4 main structures of the female pelvic floor (bladder, vagina, uterus and rectum), providing a full 3D visualization of the organs' displacements. The methodology is evaluated with two patient-specific data sets of volunteers presenting no pelvic pathology, and a sensitivity study is performed using synthetic data. The resulting simulations provide an estimation of the dynamic 3D shape of the organs facilitating diagnosis compared to 2D sequences. Moreover, the method follows a protocol compatible with current clinical constraints presenting this way potential short term medical applications.

KEYWORDS:
2D-3D Registration; Pelvic system simulation; Constraint-Based Simulation; Augmented Reality

1 | INTRODUCTION

Female genital prolapse is mainly characterized by excessive mobility of organs resulting from the weakness of the pelvic floor. It is a common pathology related to the age of women: over 60 years old, more than 60% of women suffer from it, while the average percentage is from 20% to 30% for women of all ages combined [33, 34]. According to the severity of the symptoms, surgery may be necessary. Magnetic Resonance Imaging (MRI) is often chosen for the evaluation of female pelvic pathology because this technique provides high contrast resolution without any radiation [13]. Dynamic MRI images are widely used in nowadays clinical routines [30] to capture the dynamic of organs' motion while the patient is breathing or pushing. However, the requirements of high image resolution limit the current dynamic MRI protocols to 2D slices with a frequency of acquisition between 2 and 4 images per second. Due to the limited field of view, subjectivity related to human perception as well as medical experience cannot be avoided and causes variability in the diagnoses.

Moreover, some anatomical suspension structures (ex. fasciae and ligaments) are hardly observable in MRI, but play a key role in organs' mobility [25]. As stated by recent publications [10, 25], the development of a mobility analysis tool is a major challenge to better understand the complex behavior

of organs, which is still not fully understood today, in order to provide relevant medical diagnosis and adapted surgery to cure the patient.

The contribution of this work is an automatic image-based tracking method providing the outline of organs in a set of 2D dynamic MRI images acquired during the diagnosis, that is later combined with 3D biomechanical models in order to extrapolate the complete 3D dynamic motion of structures. The ill-posed nature of the 2D/3D registration problem is reduced adding a priori knowledge of boundary conditions in order to constrain off-plane motions around the image's plane. Although the location and the mechanical properties of boundary conditions are generally not know accurately, the patient-specific data extracted from the segmentation of images are combined with generic models of suspension structures generated semi automatically thanks to previous works [25]. Contrary to pure image-based methods which generally provide information limited to images' plane, the proposed approach allows to significantly reduce the 3D displacement error, even where no data are available, allowing this way to estimate the complete kinematics of the pelvic system during the dynamic sequence.

Finally, a strong consideration was given to follow the limitations of current clinical routines in order to provide potential short term clinical applications. The resulting 3D analysis of motion allows for better identification of potential pathology.

2 | RELATED WORKS

During the last decade, patient-specific models of the pelvic system have been developed thanks to advances in experimental tests on soft tissues, mathematical modeling and computer simulations [25]. To evaluate pelvic organs' mobility Finite Element (FE) simulations have been used [37, 20], providing better understanding of the mechanisms involved in physiological or pathological cases [7, 24]. Organs' mobility is linked to mechanical properties of soft tissues, material modeling and anatomical suspension structures of the pelvic system. Indeed, [36] shows the necessity to take into account the suspension system, which is located out of the dynamic MRI plane and is rarely observed on static MRI. To improve the bio-fidelity of FE model Lecomte et al. [21] proposed a method for geometrical reconstruction based on medical imaging using dynamic MRI and digital image correlation, combined with anatomical knowledge and analysis of the measured displacement fields. However, the validity domain of the models remains limited to small deformations which prevent the method for the simulation of pathology such as prolapses involving large abnormal mobility of tissues.

As aforementioned, concerning the problems related to pelvic floor disorders, biomechanical FE models have also been involved for a proper personalized cure for pathological conditions, especially the POP (pelvic organ prolapse). Generally, applying a FE simulation requires principally the following elements : medical images providing observations and ground truth data, geometries of pelvic organs and structures, characterization of mechanical properties and definition of boundary conditions. Promising results have been made on each of these aspects. In [38], the study focused on the mechanical properties of vaginal tissue of women. The stiffness was evaluated by using a scanning haptic microscope. A comparison of tissue of women with and without POP was carried out and the relation with collagen composition was shown. [36, 37] provided useful preliminaries to the simulations of pelvic cavity behaviors. FE simulations were applied to a multi-organ model of a patient, focusing on the ligamentous boundary conditions definition. As in [12, 23, 26], more recent works proposed a solution of the three-dimensional FE modeling of the pelvic floor towards the patient-specific modeling. [26] demonstrated 3D FE simulation of the pelvic cavity under larger strain. Less complex pelvic organ models were involved in these works [12, 23], but a special attention has been paid to the patient-specific aspect and to the clinical application. Based on anatomical and surgical expertise, some important structures were turned into parameters that can be specifically defined, including the presence of muscles, hiatus size, vaginal dimension, fascia length, etc. Results were reported with respect to pelvic organ prolapse quantification system (POP-Q). In parallel with the previous contributions, [3, 16, 15] dealt with the issue of geometric modeling of pelvic organs that had not been treated in these contributions. [3] presented a method to reconstruct hollow organs with a thickness from pre-segmented points cloud. In [16], a more efficient approach was proposed to generate readily usable CAD (Computer Assisted Design) pelvic geometries for FE simulations. The geometry construction was validated by using a controlled physical model [15]. The idea is to reduce the gap in the processing pipeline from MRI to FE simulations.

Real-time registration of biomechanical models have also been used for intra-operative 3D registration with 2D dynamic MRI. In [9, 35], a model of a pig's liver is registered with 2D slices during breathing motion. Although the authors have shown that the method allows for the estimation of off-plane motions, it is limited to a single organ and requires the synchronization of 3 orthogonal slices which is not possible in a realistic clinical scenario. The methods cited above perform the registration prescribing displacements which significantly reduces the importance of both mechanical parameters and

boundary conditions of biomechanical models in the neighborhood of image's data [27]. Yet, in areas where no data are available models plays the role of a regularization term between image-based constraints [32]. In this case, the mechanical parameters as well as boundary conditions can be at least as important as the constitutive law itself [4]. Mechanical studies and rheological experiments can provide generic information about the mechanical action of boundary conditions [25]. Peterlik et al. [31] showed that the mechanical action of boundary conditions can be directly extracted from the biomechanical registration process.

This paper introduces a method for the registration of 3D FE models with material points located on the contours of organs in dynamic 2D MRI images. Compared to the previous works, this work pays more attention to the pelvic motions, using dynamic MRI as one of the ground truth data. An extensive survey can be found in [11] for 2D slices to 3D volume registration problems. A constrained-based optimization problem is solved using image features, biomechanical models, and anatomical connection. The originality of the proposed solution lies in the fact that the FE simulation is driven by image data in the plane coordinate of the 2D dynamic slices, while FE models provide an estimation of off-plane motions. The ill-posed nature of the problem is compensated by adding a priori knowledge of boundary conditions (ligaments, contacts between structures...) during the registration, providing this way a mechanical extrapolation of dynamic MRI data. Results show that adding a priori knowledge of the mechanical action of the tissues (ligaments, contacts...) allows to significantly reduce off-plane errors and provide additional information than what is observed in 2D images.

3 | EXPERIMENTAL PROTOCOL

In this section the experimental protocol allowing for acquisition of the necessary data for the simulation and the evaluation of the method is detailed. Patient-specific data are generated from two data sets of two volunteers (designed as T005 and T007 in the rest of the paper), presenting no pelvic pathology. The experimental data inputs have been acquired following a close protocol to a standard clinical routine (see Figure 1).

3.1 | Dada acquisition

Pelvic MRI requires between 20 to 50 minutes to obtain static volume images of organs (TSE) with sufficient resolution. The procedure is then immediately followed by a dynamic acquisition (DYN) while the patient is contracting and relaxing the pelvic muscles. DYN sequence is performed following the middle plane, the most representative of the organs' motion.

Data have been obtained with a 3-Tesla MR (Philips Achieva 3.0T TX) providing up to 2 images per second in a dynamic mode. Although this frequency is sufficient to capture the dynamic of tissues, the whole volume movement is not visible and its evaluation relies on the physician's experience.

TSE and DYN are already parts of standard clinical routines, but a final step (FFE) is added in order to evaluate the accuracy of the registration method. The volunteers are asked to maintain a maximal contraction of pelvic muscles without moving nor breathing. This significantly limits the time allowed for the acquisition. 15 sparse sagittal slices uniformly distributed in the volume have been acquired. Although FFE is not necessary to perform the registration, it provides the only available data to evaluate the accuracy of the method.

3.2 | Data and mesh generation

The pelvic floor is a complex system where multiple organs act together during the deformation. In this paper 4 organs are considered (Vagina, Uterus, Bladder and Rectum), whose geometries are obtained from the segmentation of TSE images (see Figure 2). Vagina and rectum are injected with gel to enhance image contrast and facilitate the segmentation procedure.

In addition to the geometries of organs, anatomical supporting structures are added in order to constrain the mobility of organs and thus provide a more realistic cinematic. The cardinal and uterosacral ligaments represent the structures maintaining the cervix and the uterus which are modeled as attached constraints to link the vagina and uterus. Paravaginal ligaments located on both sides of the vagina are also modeled to sustain the model in position and fixed at their extremities. Finally, fasciae between pelvis and bladder and the one between rectum and sacrum are taken into account. The ligaments and fasciae are not visible in the clinical images. Their geometries are obtained from anatomic literature and an iterative optimization process described in [25].

4 | TRACKING IN DYNAMIC MR IMAGES

The visible outline corresponding to each organ in the DYN MR sequence will be used to impose displacements during the simulation (Section 5.1). Nevertheless, the semi-automatic tracking of organs' outline in DYN MR images is difficult because it requires to find tangential information that cannot be obtained directly by using the image contrast. Recent works introduced a method for multiple organs detection in MR images based on B-spline model [18]. This method is used to fit an initial B-spline model for each organ at the beginning of the sequence (see Fig 3).
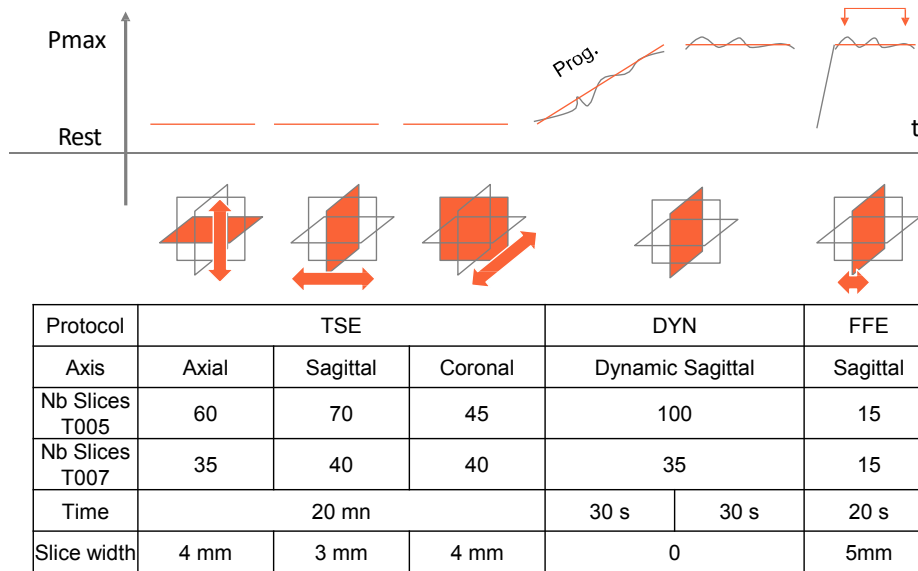
FIGURE 1 Protocol for MRI data acquisition composed of three steps. TSE: Volume acquisition is performed providing the geometry of organs. DYN: a dynamic 2D sequence is acquired during breathing and contraction of muscles. FFE: A sparse volume acquisition is performed for the validation, while the volunteer maintains a maximal pressure of organs.
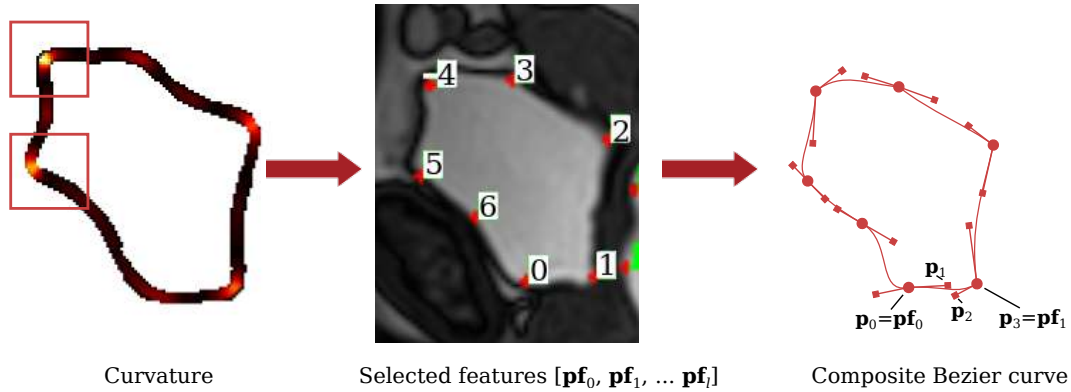

(a) Segmentation
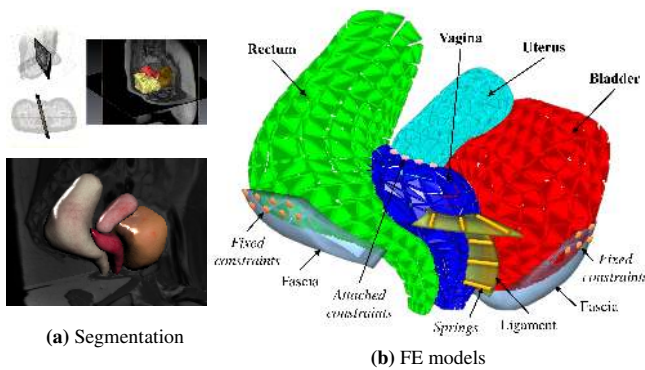
(b) FE models

FIGURE 2 Initial segmentation and meshing. (left) the segmentation is performed using TSE images. (right) FE models are generated from the segmentation and boundary condition are added to complete the FE model.

For each image, it is important to follow material points of the contour over time with maximum precautions, especially to avoid drifting along the contour boundaries. Additional feature-sensitive constraints are added in order to better track the material points and to ensure the plausibility of the computed motion [17]. These constraints consist in the detection of corner points of high curvature in order to impose normal movements of the tracked points. Based on the initial B-spline model [18], each organ is then redefined by a composite Bézier curve (a series of segments attached end to end). The beginning and ending points of Bézier segments are considered as material points, selected automatically based on the criteria of high curvature. As shown in Figure 3 , $[\mathbf{pf}_0, \mathbf{pf}_1, \cdots, \mathbf{pf}_l]$ are

the selected points. Then, the contour is deformed to fit the other images in the DYN sequence, by minimizing iteratively an energy term (more details can be found in [17]).

Figure 4 shows the semi-automatic tracking of four highlighted organs with material points: bladder (red), vagina (blue), rectum (green) and uterus (light blue). Given the poor contrast of the uterus in the image, its contour is roughly generated using optical flow. For each image i, the $2D$ points of the contour are reconstructed in $3D$ according to the slice coordinates, providing a set of points $\mathbf{m}^{(i)}$ located on the surface of each organ. With respect to the mobility of different areas, the distribution of points matches the organs shape.

During the dynamic sequence, the set of points $\mathbf{m}^{(i)}$ may not necessarily be associated with the same material points on the $3D$ surface of the models. Indeed, being located in a unique $2D$ plane position, $\mathbf{m}^{(i)}$ may represent the outline of several cross section of the organ (in case of translations or rotations of the tissues in the orthogonal direction of the image slice). Therefore, *sliding constraints* are introduced in order to prescribe displacements of biomechanical models in the plane while minimizing the mechanical energy of numerical models and to estimate the entire $3D$ displacements.

Curvature   Selected features $[\mathbf{pf}_0, \mathbf{pf}_1, \dots \mathbf{pf}_l]$ Composite Bezier curve

FIGURE 3 The tracking principle: an organ contour defined by a composite Bezier curve, the joined points (features) are selected by high curvatures. For each segment, from images t to $t + 1$, the transformation of features is computed by Optical Flow [22, 5] and the adjustment of free control points ($\mathbf{p}_1$, $\mathbf{p}_2$) is perpendicular to the segment. Such process is repeated until the end of the sequence.
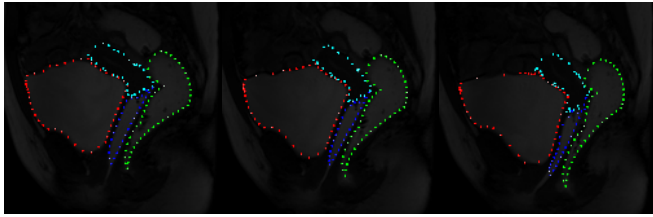
FIGURE 4 Outline tracking with material points in the sequence of dynamic MR images.

5 | CONSTRAINT-BASED REGISTRATION OF BIOMECHANICAL MODELS

FE models are meshed using linear tetrahedral elements[1], and internal forces are computed following a corotational formulation [29]. The co-rotational model was mainly used in the field of computer graphics [28], but this formulation is more and more used for medical simulations due to its low computational cost. The corotational approach is used in order to enforce the stability of the simulation and maintain computation time compatible with clinical constraints, while allowing for the simulation of large deformations.

The corotational model is parametrized with the Poisson ratio v and the young modulus E chosen for an average model in the literature (see [24] and [10] for details). The discrete formulation of elastic forces applied on the nodes of a tetrahedral element e can be written as:

$$\boldsymbol{f}_e = \mathbf{R}_e \mathbf{K}_e (\mathbf{R}_e^T \bar{\mathbf{q}}_e - \mathbf{q}_e) \qquad (1)$$

where $\bar{\mathbf{q}}_e$ and $\bar{\mathbf{q}}_e$ are respectively the initial and deformed positions of the nodes of the hexahedron and $\boldsymbol{f}_e$, the elastic forces

---

[1]Note that the method is not dependent on the type of element nor the constitutive law. For instance, surface FE models such as Thin-Shell models and hyper-elasticity could be used as employed in [25].

applied on these nodes. While $\mathbf{K}_e$ corresponds to the local linear stiffness matrix of the element, parametrized by the Young's modulus E and the Poisson's ratio v, $\mathbf{R}_e$ is a block diagonal matrix defined as:

$$\mathbf{R}_e = \begin{pmatrix} \mathbf{R} & & & \mathbf{0} \\ & \mathbf{R} & & \\ & & \mathbf{R} & \\ \mathbf{0} & & & \mathbf{R} \end{pmatrix} \qquad (2)$$

with $\mathbf{R}$ being the 3×3 rotation matrix of the tetrahedral element. The rotation matrices of each element are evaluated independently using a polar decomposition of the strain displacement, allowing this way for higher ranges of deformations.

The local stiffness matrix $\mathbf{K}_e$ can be written with the synthetic formulation:

$$\mathbf{K}_e = \mathbf{R}_e \int_{V_e} (\mathbf{C}_e \mathbf{D}_e \mathbf{C}_e \partial V_e) \mathbf{R}_e^T \qquad (3)$$
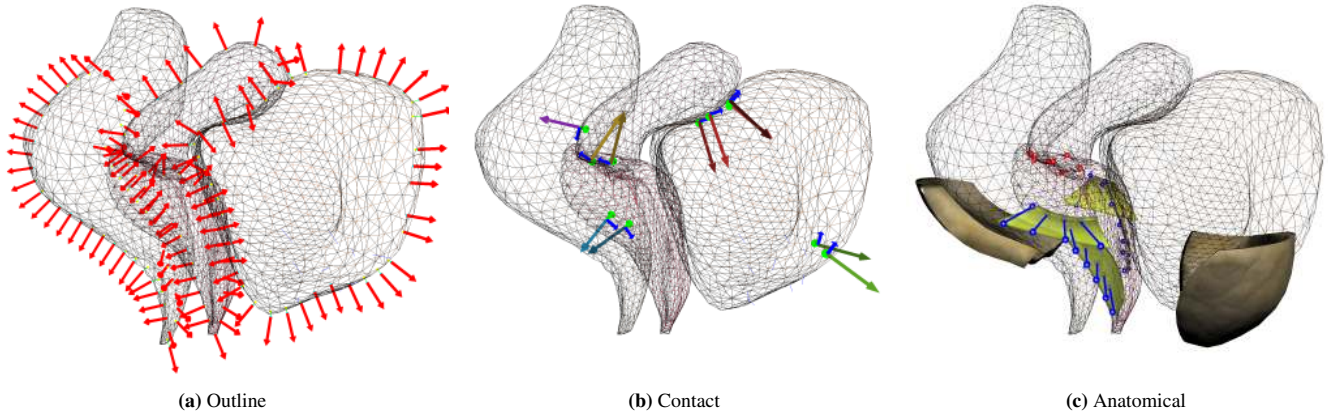
where $\mathbf{C}_e$ and $\mathbf{D}_e$ are respectively the strain-displacement matrix and the stress-strain matrix. While these matrices are constant during the simulation, $\mathbf{R}_e$ needs to be updated at each iteration providing this way a geometrically nonlinear constitutive model allowing the simulation of large displacements but small deformations.

5.1 | Constraints definition

During the simulation 3 types of constraints are used to deform the models (see Figure 5):

Sliding Constraint ω: Due to off-plan motions, control points $\mathbf{m}$ cannot be associated with constant coordinates on organs' surfaces. Therefore, to impose constraints, an Iterative Closest Point (ICP) method is used: at the beginning of each

(a) Outline   **(b)** Contact   **(c)** Anatomical

FIGURE 5 Constraints set used in the simulation: Outline constraints (left), Contact Constraints (center), Anatomical constraints (right).

simulation step, control points are associated with their respective nearest triangle on the surface of the segmented models. In addition, the ICP method is modified to enforce that the normal of the surface aim in the same direction as the normal of the contour computed in the image. Formally, Sliding Constraints are described by the following equation:

$$\omega(\mathbf{n}_s, \mathbf{q}_s, \mathbf{m}) = 0 \qquad (4)$$

where $\mathbf{m}$ are the tracked points in the 2D image and $\mathbf{q}_s$ their respective closest point on the surface of FE models. $\mathbf{n}_s$ are the associated normal of points $\mathbf{q}_s$ that are projected in the image plane in order to impose displacements in the 2D image's space and fit the outline in DYN MRI, while enforcing no orthogonal forces in 3D. This formulation allows the FE models to *slide* in the orthogonal direction and reduce the energy of the system to perform the registration (see [9] for details).

Contact Constraints ϕ: Taking into account contacts is fundamental to avoid unnatural configurations such as the interpenetration of organs outside of DYN plane. Contacts provide additional constraints that prevents unrealistic rotations of organs around the constraint DYN plane. When point contacts exist in the system, the contacts form separation distance constraints:

$$\phi(\mathbf{q}_c) \geq 0 \qquad (5)$$

which means that positions in contact $\mathbf{q}_c$ of FE models must remains on the positive side of the surface normals. A volume-based method relying on the computation of Layered Depth Images (LDI) (see [1] for details) is used to perform the collision detection between structures. Volume-based methods are robust to deep intersections, which are unavoidable due to data noise and approximations in the reconstruction process. Friction is also added to prevent large lateral motion between organs due to the presence of connective tissues.

Anatomical Constraints χ: Anatomical constraints are added to limit the off-plane motion of organs (see Figure 5 c). The vagina is attached at each side by ligaments reconstructed semi-automatically using the method introduced in [25] and meshed with regular hexahedral elements. Bilateral constraints are added between the vagina and ligaments allowing the vertical mobility but penalizing lateral motions. The uterus is attached to the vagina with bilateral constraints (red), linking the displacement of both structures. These constraints can be formalized with:

$$\chi(\mathbf{q}_v, \mathbf{q}_u) = 0 \qquad (6)$$

where $\mathbf{q}_v$ and $\mathbf{q}_u$ are the attached positions of the vagina and uterus. In addition, fasciae constrain lateral motions of the bladder and the rectum on each side. Since these structures are not visible in the images, their precise location and geometries are not known and may change during the sequence. In order to avoid the generation of unsolvable problems where the outline of the organs overlaps the initial geometries of faciae during the dynamic motion, these structures are considered deformable with fixed constraints on their extremity. Faciae are attached to the rectum and the bladder with bilateral constraints remaining this way in contact with tissues while deformations allow satisfying images constraints.

While ω are derived from visible images' data and used to drive models, other constraints are instead added as a-priori knowledge of organs' behavior to prevent unrealistic behaviors (such as interpenetration) and reduce the number of solutions of the ill-posed $2D/3D$ registration problem.

5.2 | Solving Process

For each DYN MR image (every 0.25 sec in average), a static problem is solved to find equilibrium between internal

elastic forces and constraint forces applied to satisfy image data. Nevertheless, a dynamic formulation is chosen to integrate the simulation models over time. Indeed, even if the motion is prescribed within the MRI plane (where dynamic is already provided by images), off plane displacements are entirely driven by the models where dynamic is necessary. In addition, dynamic integration allows stabilizing the problem and in the absence of external forces, it incrementally iterates toward a static equilibrium solution.

FE's governing equation is given by the following dynamic equations:

$$\mathbf{M}\ddot{\mathbf{q}} + \mathcal{F}(\mathbf{q}) + \mathcal{H}(\mathbf{q}, \mathbf{m}^{(i)})\lambda = \mathbf{0} \qquad (7)$$

where $\mathcal{F}(\mathbf{q})$ are internal volume forces (given by the co-rotational formulation, which corresponds to equation (1).) depending on positions $\mathbf{q}$ and velocities $\dot{\mathbf{q}}$ of FE models. $\mathbf{M}$ is the mass matrix used to integrate the dynamic of the system and numerically stabilize the system. The mass of organs are parametrized according to the literature[2]. $\mathcal{H}(\mathbf{q}, \mathbf{m}^{(i)})$ is a non-linear function gathering the set of constraints applied on the models ω, ϕ and χ. This function takes as input $\mathbf{q}$ and $\mathbf{m}^{(i)}$ which are, respectively, the position of the FE models and the set of points extracted from an image i and reconstructed in 3D. Its formulation is linearized at each simulation step (see below). Lagrange multipliers λ are used to impose the constraints.

For each simulation step, the nodal velocities $\dot{\mathbf{q}}$ and nodal positions $\mathbf{q}$ are updated following a backward Euler Implicit method. The nodal accelerations $\ddot{\mathbf{q}}$ at the end of the time step t are given by $\dot{\mathbf{q}}_{t+h} = \dot{\mathbf{q}}_t + h\,\ddot{\mathbf{q}}_{t+h}$ and $\mathbf{q}_{t+h} = \mathbf{q}_t + h\,\dot{\mathbf{q}}_{t+h}$, where h is the simulation time step. Yet, since several images are acquired per second in the DYN sequence, very small displacements are observed between images, and dynamic effects in the image plane remains limited. h is mainly used as a parameter to control the number of iterations of the iterative solver described below, and it does not influence the converged configurations of the models.

Since $\dot{\mathbf{q}}_{t+h}$ and $\mathbf{q}_{t+h}$ are unknown, the non-linear problem defined in equation (7) is linearized (equivalent to a first order Taylor expansion). Assuming that no constraints λ are applied at the beginning of each simulation step t (i.e. $\lambda_t = \mathbf{0}$, see [27] for details) it gives:

$$\left[\frac{1}{h}\mathbf{M} + h\left.\frac{\partial \mathcal{F}}{\partial \mathbf{q}}\right|_{\mathbf{q}_t}\right](\mathbf{q}_{t+h} - \mathbf{q}_t) = -\mathcal{F}(\mathbf{q}_t) \qquad (8)$$

In addition, constraint equations, are linearized at the beginning of each simulation step and assumed constant during the

time step. It can be written as follows:

$$\mathbf{H}^T(\mathbf{q}_{t+h} - \mathbf{q}_t) = \delta, \quad \text{with } \mathbf{H} = \left[\left.\frac{\partial \mathcal{H}_\omega}{\partial \mathbf{q}}\right|_{\mathbf{q}_t}; \left.\frac{\partial \mathcal{H}_\phi}{\partial \mathbf{q}}\right|_{\mathbf{q}_t}; \left.\frac{\partial \mathcal{H}_\chi}{\partial \mathbf{q}}\right|_{\mathbf{q}_t}\right] \qquad (9)$$

where $\mathbf{H}$ is known as the *Jacobian of the constraints*. This matrix includes both the direction in which the contact forces λ are applied and the *Degrees of Freedom* of the models impacted by the constraints to cancel the penetration δ. These directions are obtained either from the ICP method (for ω constraints) or from the collision detection (for contact constraints).

The combination of the non-linear constraint equations, provides a KKT (Karush-Kuhn-Tucker) problem:

$$\begin{cases} \mathbf{A}\mathbf{x} + \mathbf{H}\lambda &= \mathbf{b} \\ \mathbf{H}^T\mathbf{x} &= \delta \end{cases} \qquad (10)$$

where $\lambda, \mathbf{x} = (\mathbf{q}_{t+h} - \mathbf{q}_t)$ and δ are unknown; $\mathbf{b} = -\mathcal{F}(\mathbf{q}_t)$ and $\mathbf{A} = \frac{1}{h}\mathbf{M} + h\left.\frac{\partial \mathcal{F}}{\partial \mathbf{q}}\right|_{\mathbf{q}_t}$ (see [8] for details).

The Schür complement method is used to solve the augmented linear system, involving the computation of the *compliance matrix* $\mathbf{W} = \mathbf{H}\mathbf{A}^{-1}\mathbf{H}^T$ that relates the mechanical coupling between constraints. This matrix is computed in real-time with GPU parallelization as details in [8].

The constraint problem is solved with an iterative Gauss-Seidel algorithm which allows for fast definition of non-linear contact forces (such as friction). More importantly the iterative solver provides stable solutions even in case of non-convergence of the solver. Indeed, since most of our constraints depend either on image data or specific simulated positions (for the ICP); it is difficult to guarantee the well-posedness of the constraint problems. This may result in redundant or even antagonist constraints which prevent the use of direct solvers.

6 | RESULTS

Based on patient-specific data, the evaluation of the method is limited to the fact there are no imaging modalities allowing retrieving the complete 3D displacements of organs during the registration process. Therefore, after introducing the mesh generation procedure, a synthetic evaluation of the method is described providing quantitative results of the dynamic 3D motion. Then the method is applied to the patient specific data described above. The 15 FFE Sagittal images have been segmented manually providing a coarse representation of the organs' geometries at maximal pressure state (see Figure 8 a). The evaluation of the method is compared to the ground truth at the final state of the dynamic acquisition using manually segmented positions in the FFE slices.

---

[2]note that mass parameters do not have any influence at equilibrium state since no gravity is applied

6.1 | Mesh generation

Real-time FE models have been generated and integrated in Sofa[3] (see table 1). Since the considered organs are membranous structures, hollow tetrahedral FE models were generated from an extrusion of a constant thickness of their surface allowing this way for compression with high resistance in elongation, except for the uterus which is discretized with a full volume of tetrahedral elements. In addition, the ligaments and fascia, are not visible in the clinical images. Specific FE models have been generated semi-automatically (see [24]) and meshed with regular grids of hexahedral elements. These supporting structures are considered fixed at their extremities, far from the interactions with the other organs.

	DoF (T005)	DoF (T007)	E (MPa)
Vagina	928	1789	0.66
Uterus	740	523	0.6
Bladder	806	772	0.24
Rectum	894	2205	0.54
Fascia Pelvis	170	352	0.03
Fascia Sacrum	288	326	0.03
Ligaments	199	233	0.78

TABLE 1 Number of degrees of freedom (DoF) and Young's modulus (E) of the FE models used for the registration.

The characterization of pelvic tissues has been extensively studied [2]. Yet, mechanical parameters in patient specific scenarios are subject to variability. Therefore, all the following simulations have been run 100 times, where the mechanical parameters of each model have been randomized within a range of 10% around the values given in the table 1 . The following results include the average error and the standard deviation of this simulations set.

6.2 | Synthetic evaluation

A numerical FE simulations have been performed on Abaqus software using the data of the patient T005. The convergence of the FE simulation, as well as a mesh sensitivity, was carried out in order to guarantee the validity of the results. The hyperelastic behavior of the soft tissues of the pelvic system is taken into account thanks to previous published works [6]. We assume that the material is homogeneous. Based on the semi-automatic detection on MRI [16], a FE model is generated thanks to shell elements for the organs (vagina, bladder, rectum) and pelvic floor [26]. Ligaments are also considered with truss elements to mimic the sustainable structures, as they

play a key role in the organ's mobility [12]. The average displacement of the vagina was 8.2 mm in the dynamic image plane. Although the displacement is small compared to medical data, this simulation provides the complete 3D motion of structures allowing this way to obtain quantitative evaluations of the accuracy of the registration during the dynamic process.

Nodal displacements of meshes in the Abaqus simulation have been exported for 15 simulation steps, allowing this way to generate both the ground truth and similar input data as described in the experimental protocol of the section 3. Each position is then successively played during 3 simulation steps in Sofa while performing the registration. For this purpose, the outline of organs was generated from the intersection of Abaqus' models and the image plane coordinates of the 2D dynamic MRI sequence. These positions are used to impose displacements of meshes in Sofa.

Figure 6 (top) reports the average distance between positions extracted in Abaqus (uniformly sampled every 5 mm over the complete surface of organs) and the closest surface triangle of the registered models for the complete process; while taking into account or not (left/right) the boundary conditions. Even if models are only driven by a set of constraints located in a single plane, the registration procedure allows maintaining an average error smaller than 4 mm over the entire 3D volume for any deformation step. In addition, the error of the vagina is reduced by a factor 2 when taking into account the suspension structures and boundary conditions, allowing this way for the complete 3D extrapolation of off-plane motion. In addition, Figure 6 (bottom) shows the average error at the final state (step 45) measured as the intersection of organs' surfaces with the 15 FFE slices acquired in the medical data[4]. As expected, the error is minimal at the location where constraints are imposed (index 0). However, the error remains small for all the other slices located both sides side of the constraint slice (positive and negative indexes). In addition, although the method provides similar accuracy results in the dynamic plane, error increases significantly faster when boundary conditions are not taken into account. This is because the off-plane motion results in non-realistic rotations of organs around the constrained plane.

The numerical simulation in Abaqus relies on small perturbations theory and only focuses on the movement at the beginning of motion to ensure numerical stability. In order to evaluate the accuracy of method with larger motion, FE models have been registered with the set of tracked positions obtained in the dynamic MRI slice (see section 4). The accuracy of the registration with respect to medical data will be detailed in the next section. Instead, the generated motion is first used
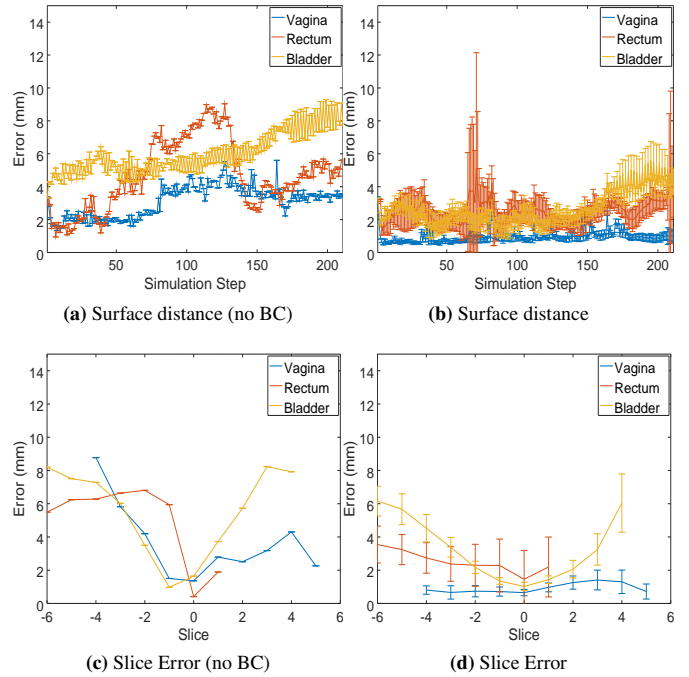
---

[3]https://www.sofa-framework.org

[4]Note that the 3D geometry of organs does not necessarily cross all the validation slices and does not necessarily have values for all the columns in the graphs.

(a) Surface distance (no BC) **(b)** Surface distance

(c) Slice Error (no BC) **(d)** Slice Error
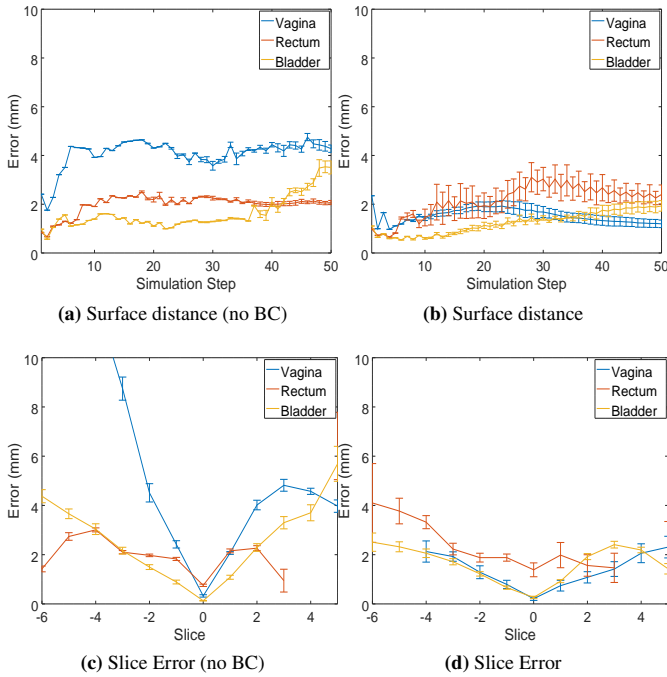
FIGURE 6 Evaluation of the registration method using the simulation generated with Abaqus.

(a) Surface distance (no BC) **(b)** Surface distance

(c) Slice Error (no BC) **(d)** Slice Error

FIGURE 7 Evaluation of the registration method using the simulation generated with Sofa.

to perform a sensitivity study of the method with respect to mechanical parameters.

During the dynamic sequence, the maximal displacement of the vagina was measured above 2.5 cm. Figure 7 reports the errors of the proposed solution with this data set. As previously, the method allows maintaining a small distance between the simulated surfaces and the registered shapes. However, in this scenario the importance of anatomical constraints is enhanced since it allows to reduce the average error by a factor 4× for the vagina and 2× for the other organs. More importantly, when boundary conditions are not simulated, the standard deviation related to the uncertainty of mechanical parameters is almost null because image-based constraints ω does not depend on the mechanical parameters but only on the geometry of the models. Therefore, the resulting deformations always converge to similar situations, providing higher errors, without taking into account the mechanical behavior of structures. When adding the boundary conditions, the method still provides reproducible results (small standard deviation) independently of the chosen parameters within the range of variability. Finally, similar conclusions are obtained at the final step when the errors are measured independently for each validation slice (FFE), i.e. the error increase significantly faster with respect to the distance of the constraint plane, when boundary conditions are not taken into account.

6.3 | Patient-specific application

The method has been applied with the two patient-specific data of the volunteers. An overlapping with the organs' geometries at the final state is shown in Figure 8 . Results show that complex motion and deformations happened, enhancing the need for biomechanical models during the registration: For T005 the vagina has been significantly displaced and contracted, leading to the compression of the rectum and sliding of the uterus along the bladder. For T007, the bladder is compressed by surrounding tissues and the fasciae which result in a significant modification of the geometry of the organ. Our method provides realistic transitions including far from the image plane.

The average distance error according to FFE segmentation is reported in Figure 9 . Results show that our biomechanical registration allows to significantly reduce the error in the 2D DYN plane (index 0) where constraints are applied, but it can also provide an accurate extrapolation for off-plane motion. The vagina undergoes the most important displacement where an average error between TSE and FFE surfaces are initially around 15*mn* and reduced to 3*mm* using our method. A possible explanation of the remaining error can be related to the significant amount of contrast gel expelled during the dynamic acquisition (due to compression of muscles) which is not taken into account in current FE models. As observed with synthetic data, boundary conditions allow not only to decrease the off-plane errors far from the image constraint, but they also prevent

(a) T005 FFE   **(b)** T005 TSE   **(c)** T005 FFE

(d) T007 FFE   **(e)** T007 TSE   **(f)** T007 FFE
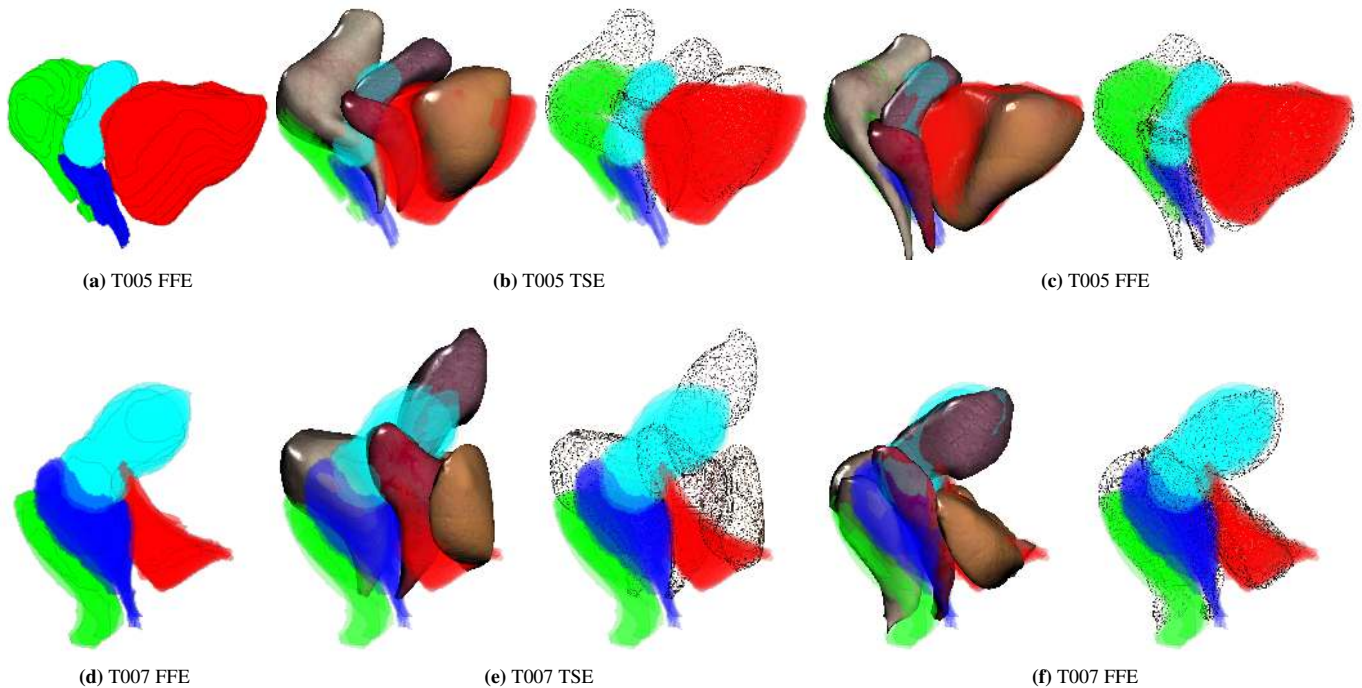
FIGURE 8 Overlapping between sparse FFE segmentation (8 a) and organs' geometries for both before (8 b) and after (8 c) the dynamic registration.

the simulated models to produce unrealistic and non-physically possible configurations such as rotations of organs around the constrained plane or inter-penetrations.

Finally, despite the complex interactions and the high number of degrees of freedom, all the above simulations achieved a fixed frame rate of 14 frames per second with data T005 and 8 FPS with T007 on an Intel(R) Core(TM) i9-9900K CPU @ 3.60GHz and a GeForce RTX 2070. Each simulation step involves on average 30 non-linear friction contact constraints with 70 outline constraints. Given the acquisition time of the MRI, the frame rate it is sufficient to perform real-time simulation of the MRI sequence (i.e. 1 second can be simulated in 1 second). Therefore, apart from the segmentation and meshing of TSE images, this method open the possibility of real-time diagnosis and planning of the future surgery. Indeed, the real-time computation offer the possibility to evaluate the influence of mechanical structures and the effect of boundary conditions for future planning assistance of the surgery.
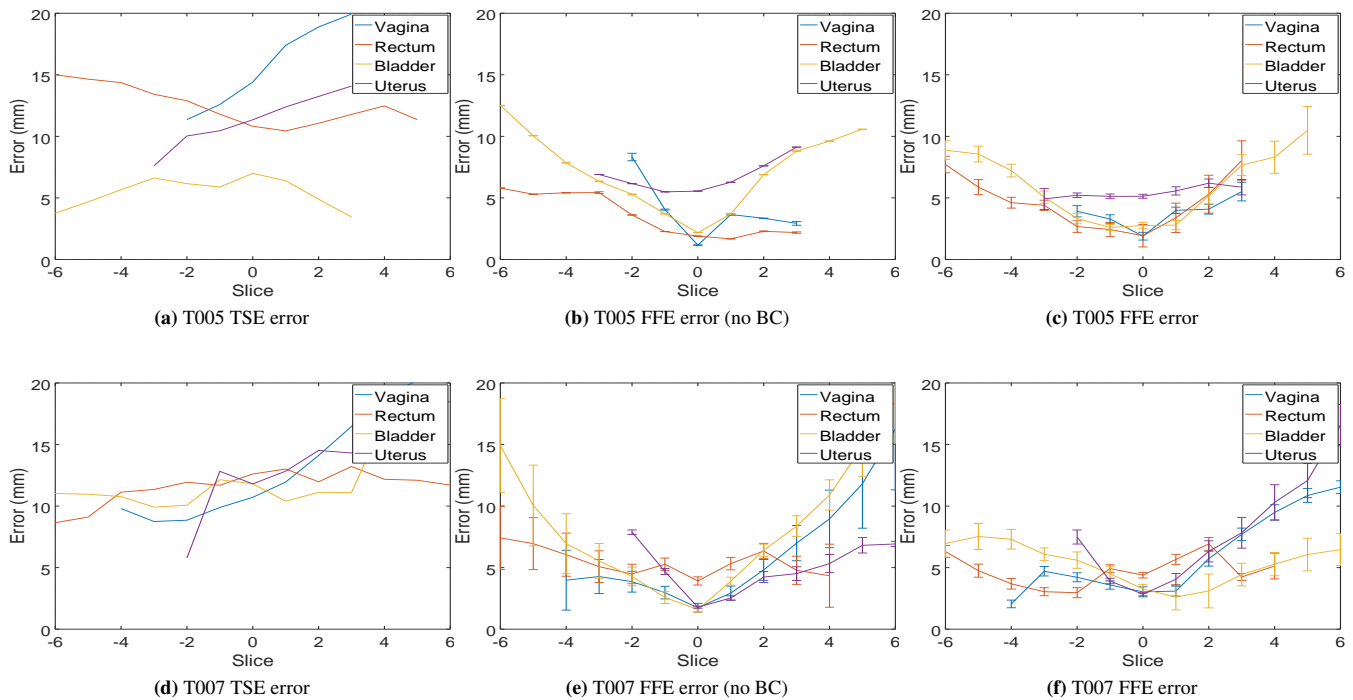
7 | CONCLUSION AND DISCUSSION

A method for semi-automatic registration of pelvic organs has been proposed which is compatible with nowadays clinical routines. The method relies on the registration of 3D FE models to 2D dynamic MRI slices, providing a biomechanical extrapolation for off-plane dynamic motion of organs.

The method has been validated with patient specific data of two volunteers. This approach allows moving towards the patient-specific treatment. Indeed, this work based on medical imaging and numerical simulation would make it possible to better understand pelvic mobility and to study the potential defects related to the equilibrium of pelvic statics [19]. The care can be adapted more precisely to the pathology in a specific way using a numerical FE model. The method leads to interesting results linking medical imaging process to the definition of the pelvic organs mobility and the stress-strain equilibrium. Understanding the impact of surgical techniques to treat the patient is essential for the development of more effective surgical prolapse repair [14]. Numerical simulations of the organ's mobility allow to advance our knowledge on the impact of various surgical techniques and to improve surgical decision-making on the choice of techniques, by considering the mobility of organs with this method. Moreover, preoperative simulation could enable the results of a surgical procedure to be predicted and the technique to be adapted to the individual patient.

References

[1] Allard, J., F. Faure, H. Courtecuisse, F. Falipou, C. Duriez, and P. Kry, 2010: Volume Contact Constraints at Arbitrary Resolution. *ACM Transactions on*

(a) T005 TSE error

(b) T005 FFE error (no BC)

(c) T005 FFE error

(d) T007 TSE error

(e) T007 FFE error (no BC)

(f) T007 FFE error

FIGURE 9 Average distance error (mm) according to the index of FFE Sagittal planes. Index 0 corresponds to the location of DYN slices (i.e. where constraints are applied).

Graphics, **29**, no. 3.

[2] Baah-Dwomoh, A., J. McGuire, T. Tan, and R. De Vita, 2016: Mechanical Properties of Female Reproductive Organs and Supporting Connective Tissues: A Review of the Current State of Knowledge. *Applied Mechanics Reviews*, **68**, no. 6, 060801.

[3] Bay, T., J.-C. Chambelland, R. Raffin, M. Daniel, and M.-E. Bellemare, 2011: Geometric modeling of pelvic organs. *Conference proceedings : ... Annual International Conference of the IEEE Engineering in Medicine and Biology Society. IEEE Engineering in Medicine and Biology Society. Annual Conference*, **2011**, 4329–4332, doi:10.1109/IEMBS.2011.6091074. URL http://www.ncbi.nlm.nih.gov/pubmed/22255297

[4] Bosman, J., N. Haouchine, J. Dequidt, I. Peterlik, S. Cotin, and C. Duriez, 2014: The Role of Ligaments: Patient-Specific or Scenario-Specific ? *International Symposium on Biomedical Simulation ISBMS*, Strasbourg, France.

[5] Brox, T. and J. Malik, 2011: Large displacement optical flow: descriptor matching in variational motion estimation. *IEEE Transactions on Pattern Analysis and Machine Intelligence*, **33**, no. 3, 500–513.

[6] Chantereau, P., M. Brieu, M. Kammal, J. Farthmann, B. Gabriel, and M. Cosson, 2014: Mechanical properties of pelvic soft tissue of young women and impact of aging. *International Urogynecology Journal*, **25**, no. 11, 1547–1553.

[7] Chen, L., J. A. Ashton-Miller, and J. O. L. DeLancey, 2009: A 3d finite element model of anterior vaginal wall support to evaluate mechanisms underlying cystocele formation. *Int. J. Biomech.*, **42**, no. 10, 1371–1377.

[8] Courtecuisse, H., J. Allard, P. Kerfriden, S. P. A. Bordas, S. Cotin, and C. Duriez, 2014: Real-time simulation of contact and cutting of heterogeneous soft-tissues. *Medical Image Analysis*, **18**, no. 2, 394–410.

[9] Courtecuisse, H., I. Peterlík, R. Trivisonne, C. Duriez, and S. Cotin, 2014: Constraint-Based Simulation for Non-Rigid Real-Time Registration. *MMVR*.

[10] Egorov, V., H. Van Raalte, and V. Lucente, 2012: Quantifying vaginal tissue elasticity under normal and prolapse conditions by tactile imaging. *International Urogynecology Journal and Pelvic Floor Dysfunction*, **23**, no. 4, 459–466.

[11] Ferrante, E. and N. Paragios, 2017: Slice-to-volume medical image registration: A survey. *Medical Image Analysis*, **39**, 101 – 123.

[12] Gordon, M. T., J. O. L. DeLancey, A. Renfroe, A. Battles, and L. Chen, 2019: Development of anatomically based customizable three-dimensional finite-element model of pelvic floor support system: Pop-sim1.0. *Interface Focus*, **9**, no. 4, 20190022.

[13] Hamm, B. and R. Forstner, Eds., 2007: *Diagnostic Imaging - MRI and CT of the Female Pelvis*. Diagnostic Imaging, Springer-Verlag Berlin Heidelberg.

[14] Jeanditgautier, E., O. Mayeur, M. Brieu, G. Lamblin, C. Rubod, and M. Cosson, 2016: Mobility and stress analysis of different surgical simulations during a sacral colpopexy, using a finite element model of the pelvic system. *International Urogynecology Journal*, **27**, no. 6, 951–957.

[15] Jiang, Z., O. Mayeur, L. Patrouix, D. Cirette, J.-F. Witz, J. Dumont, and M. Brieu, 2020: Patient-specific modeling of pelvic system from mri for numerical simulation: Validation using a physical model. *Computational Biomechanics for Medicine*, M. P. Nash, P. M. Nielsen, A. Wittek, K. Miller, and G. R. Joldes, Eds., Springer International Publishing, Cham, 19–30.

[16] Jiang, Z., O. Mayeur, J.-F. Witz, P. Lecomte-Grosbras, J. Dequidt, M. Cosson, C. Duriez, and M. Brieu, 2019: Virtual image correlation of magnetic resonance images for 3d geometric modelling of pelvic organs. *Strain*, **55**, no. 3, e12305, doi:10.1111/str.12305.

[17] Jiang, Z., J.-F. Witz, P. Lecomte-Grosbras, J. Dequidt, S. Cotin, C. Rubod, C. Duriez, and M. Brieu, 2017: Multiorgan motion tracking in dynamic magnetic resonance imaging for evaluation of pelvic system mobility and shear strain. *Strain*, **53**, no. 2, e12224.

[18] Jiang, Z., J. F. Witz, P. Lecomte-Grosbras, J. Dequidt, C. Duriez, M. Cosson, S. Cotin, and M. Brieu, 2015: B-spline based multi-organ detection in magnetic resonance imaging. *Strain*, **51**, no. 3, 235–247.

[19] Lamblin, G., O. Mayeur, G. Giraudet, E. JeanditGautier, G. Chene, M. Brieu, C. Rubod, and M. Cosson, 2016: Pathophysiological aspects of cystocele with a 3d finite elements model. *Archives of Gynecology and Obstetrics*, **294**, no. 5, 983–989.

[20] Lecomte-Grosbras, P., M. Nassirou - Diallo, J.-F. Witz, D. Marchal, J. Dequidt, S. Cotin, M. Cosson, C. Duriez, and M. Brieu, 2013: Towards a better understanding of pelvic system disorders using numerical simulation. *Medical Image Computing and Computer Assisted Intervention - MICCAI. Nagoya, Japan*, **16**, no. Pt 3, 307–314.

[21] Lecomte-Grosbras, P., J.-F. Witz, M. Brieu, N. Faye, M. Cosson, and C. Rubod, 2015: Quantification of pelvic mobility on dynamic magnetic resonance images: Using mechanical insight to help diagnose pelvic pathologies. *Strain.*, **51**, no. 4, 301–310.

[22] Lucas, B. D. and T. Kanade, 1981: An iterative image registration technique with an application to stereo vision. *IJCAI*, volume 81, 674–679.

[23] Luo, J., L. Chen, D. E. Fenner, J. A. Ashton-Miller, and J. O. L. DeLancey, 2015: A multi-compartment 3-d finite element model of rectocele and its interaction with cystocele. *Journal of Biomechanics*, **48**, no. 9, 1580 – 1586.

[24] Mayeur, O., G. Lamblin, P. Lecomte-Grosbras, M. Brieu, C. Rubod, and M. Cosson, 2014: FE Simulation for the Understanding of the Median Cystocele Prolapse Occurrence. *Biomedical Simulation*, 220–227.

[25] Mayeur, O., J. F. Witz, P. Lecomte-Grosbras, M. Brieu, M. Cosson, and K. Miller, 2016: Influence of Geometry and Mechanical Properties on the Accuracy of Patient-Specific Simulation of Women Pelvic Floor. *Annals of Biomedical Engineering*, **44**, no. 1, 202–212.

[26] Mayeur, O., J.-F. Witz, P. Lecomte-Grosbras, M. Cosson, and M. Brieu, 2019: Patient-specific simulation: Non-destructive identification method for soft tissue under large strain: Application to pelvic system. *Computational Biomechanics for Medicine*, P. M. F. Nielsen, A. Wittek, K. Miller, B. Doyle, G. R. Joldes, and M. P. Nash, Eds., Springer International Publishing, Cham, 131–144.

[27] Morin, F., H. Courtecuisse, I. Reinertsen, F. Le Lann, O. Palombi, Y. Payan, and M. Chabanas, 2017: Brain-shift compensation using intraoperative ultrasound and constraint-based biomechanical simulation. *Medical Image Analysis*, **40**, 133–153, doi:10.1016/j.media.2017.06.003.

[28] Müller, M., J. Dorsey, L. McMillan, R. Jagnow, and B. Cutler, 2002: Stable real-time deformations. *Proceedings of the 2002 ACM SIGGRAPH/Eurographics symposium on Computer animation - SCA '02*, ACM Press, New York, New York, USA, 49.

[29] Müller, M. and M. Gross, 2004: Interactive virtual materials. *GI '04: Proc. of Graphics Interface 2004*, School of Computer Science, University of Waterloo, Waterloo, Ontario,Canada, 239–246.

[30] Pannu, H. K., H. S. Kaufman, G. W. Cundiff, R. Genadry, D. A. Bluemke, and E. K. Fishman, 2000: Dynamic MR imaging of pelvic organ prolapse: Spectrum of abnormalities 1. *Radiographics*, **20**, no. 6, 1567–1582.

[31] Peterlik, I., H. Courtecuisse, C. Duriez, and S. Cotin, 2014: Model-Based Identification of Anatomical Boundary Conditions in Living Tissues. *Information Processing in Computer Assisted Interventions*, Fukuoka, Japan.

[32] Peterlik, I., H. Courtecuisse, R. Rohling, P. Abolmaesumi, C. Nguan, S. Cotin, and S. E. Salcudean, 2017: Fast Elastic Registration of Soft Tissues under Large Deformations. *Medical Image Analysis*.

[33] Samuelsson, E. C., F. T. Arne Victor, G. Tibblin, and K. F. Svärdsudd, 2015: Signs of genital prolapse in a Swedish population of women 20 to 59 years of age and possible related factors. *American Journal of Obstetrics & Gynecology*, **180**, no. 2, 299–305.

[34] Swift, S. E., 2015: The distribution of pelvic organ support in a population of female subjects seen for routine gynecologic health care. *American Journal of Obstetrics & Gynecology*, **183**, no. 2, 277–285.

[35] Trivisonne, R., I. Peterlik, S. Cotin, and H. Courtecuisse, 2016: 3D Physics-Based Registration of 2D Dynamic MRI Data. *MMVR - Medicine Meets Virtual Reality*, Los Angeles, United States.

[36] Vallet, A., C. Rubod, J.-F. Witz, M. Brieu, and M. Cosson, 2011: Simulation of pelvic mobility: topology optimisation of ligamentous system. *CMBBE*, **14**, no. sup1, 161–162.

[37] Venugopala Rao, G., C. Rubod, M. Brieu, N. Bhatnagar, and M. Cosson, 2010: Experiments and finite element modelling for the study of prolapse in the pelvic floor system. *Computer methods in biomechanics and biomedical engineering*, **13**, no. 3, 349–357.

[38] Zhou, L., J. Lee, Y. Wen, C. Constantinou, M. Yoshinobu, S. Omata, and B. Chen, 2012: Biomechanical properties and associated collagen composition in vaginal tissue of women with pelvic organ prolapse. *Journal of Urology*, **188**, no. 3, 875–880.